Institution of MECHANICAL ENGINEERS

Journal of RAIL AND RAPID TRANSIT

Identification of a wheel–rail adhesion coefficient from experimental data during braking tests

Monica Malvezzi[1], Luca Pugi[2], Susanna Papini[2], Andrea Rindi[2] and Paolo Toni[2]

Abstract
The forces that occur in the wheel–rail interface significantly affect vehicle dynamics, especially in the longitudinal direction. Conventionally, the tangential component of the force exchanged between the rail and the wheel is expressed as the product of the normal component of the force, and the so-called adhesion coefficient. This ratio depends on several parameters that are usually summarized in the term 'adhesion conditions'. When the adhesion conditions are degraded (for example, in cases of rain, fog, ice, dead leaves, etc.), and the vehicle is accelerating or braking, pure rolling conditions between the wheels and the rails do not hold any more, and macroscopic sliding occurs on one or more of the wheels. The aim of this work is to identify a relationship between adhesion coefficient and some parameters, namely wheel sliding and train speed, starting from a set of experimental measurements, obtained from test runs conducted with artificially degraded adhesion conditions.

Introduction

The contact between wheels and rails is very important in the dynamic behaviour of railways vehicles, and has been studied since the very beginning of railways. The resultant of the pressure distribution that arises in the contact patch can be represented by a force and a resultant moment (spin). The resulting force can be expressed as the vectorial sum of one component tangent to the wheel in the contact point and another component normal to the wheel profile in the same point. By increasing the tangential force starting from zero, and fixing the remaining relevant parameters, two different phases can be distinguished.

The first one, named pseudo-sliding, mainly depends on elastic deformation of the two contact bodies. In this case, the contact area can be divided into two zones, in the first zone, relative slip between the bodies occurs, while the second zone is characterized by the adhesion between contact surfaces.[1,2] The overall size of the contact patch depends substantially on the normal component of the contact force, while the relative dimensions between sliding and adhesion areas depend on the ratio between the tangential and normal components of the contact forces. The tangential component of the force exchanged between the wheel and the rail is given by the integral of the tangential stresses

that arise in the slip zone. With growing longitudinal forces the adhesion zone decreases up to a limit situation where sliding occurs on the whole contact area. This is the second phase, that may occur during braking and traction operations and when adhesion between the wheel and the rail is poor. In such situations, the adhesion coefficient is a function of several parameters (normal load, sliding speed, temperature of the two bodies, contact geometry, weather conditions, presence of rain, snow, dead leaves, etc.), and the dependency on some of them may not be easily expressed analytically.

The adhesion coefficient μ, conventionally defined as the ratio between the tangential and the normal component of the force exchanged between the wheel and the rail (respectively T and N), is expressed as

$$\mu = \frac{T}{N} \tag{1}$$

[1]Department of Information Engineering, University of Siena, Italy
[2]MDM Lab., Energy Department, University of Florence, Firenze, Italy

Corresponding author:
Monica Malvezzi, Department of Information Engineering, University of Siena, via Roma 56, Siena, 53100, Italy.
Email: malvezzi@dii.unisi.it

The coefficient μ depends on several uncontrollable and difficult to quantify factors, and the research of a law that relates it to other directly measurable variables (train speed, wheel velocity, etc.) is a difficult task. Some experimental identification procedures of wheel–rail contact forces are presented in the literature.[3–10] On the other hand, the definition of a wheel–rail interaction model is needed for the realization of a 'real-time' realistic simulator of the dynamic of a railway vehicle, which will be used to test in laboratory 'runs' (by means of properly designed test rigs) the behaviour of on-board devices that are part of advanced train control and monitoring systems, thus reducing the cost of line tests, such as automatic train protection and automatic train control (ATP/ATC) on-board elements, wheel slide protection (WSP) systems, anti-slip devices and so on.[11] More complex test rigs are necessary to test the interaction between different on-board subsystems also in critical conditions: in particular virtual test runs with degraded adhesion conditions may be used for hardware-in-the-loop testing of the complex interactions arising between different on-board subsystems on scaled[12] or full-scale roller rigs.[13]

A quantitative and reliable model of the wheel–rail interaction forces is needed also to design and develop innovative devices (for example, WSP and anti-skid devices), in particular, to test, by means of software simulations, the behaviour of innovative control strategies. In this paper, the identification of the wheel–rail adhesion coefficient starting from experimental measurements is described. In particular, research has been performed with the goal of obtaining a reliable and computationally efficient model of the wheel–rail contact to be used in a hardware-in-the-loop simulator of the dynamics of a railway vehicle, devoted to test WSP and odometry systems.

The paper is organized as follows: in the next section , a brief introduction to wheel–rail interactions during degraded adhesion tests is presented. Then, the experimental data and corresponding vehicle model are described; a simplified dynamic model adopted to identify adhesion coefficient from experimental data is presented; the proposed identification model based on feed-forward neural networks is presented; the results of the training and validation on available experimental data are shown; and finally the results obtained are discussed.

Problem description

The adhesion coefficient, introduced in the preceding section, depends on a large number of variables: environmental conditions (e.g. presence of water, snow, ice on the rail surface), materials, temperature, etc. Due to the complexity of the phenomenon, with constant environmental conditions, it is commonly accepted to express adhesion as a function of sliding speed, Δv, defined as the difference between the vehicle speed and the tangential velocity of the wheel at the point of contact,[6,14,15] defined as

$$\Delta v = v - r\omega \tag{2}$$

in a *braking* phase, and

$$\Delta v = r\omega - v \tag{3}$$

in a *traction* phase. where v is the vehicle speed, ω is the angular wheel velocity and r is the wheel contact radius.

As will be explained in the following subsection, in the so-called pseudo-slip or *creepage* zone, i.e. the part of the adhesion curve where the sliding between the wheel and the rail is *small*, and the elastic deformations of the bodies determine the entity of the tangential force exchanged, the adhesion coefficient depends on the relative slip,[1,2] given by the following expression

$$\delta v = \frac{v - r\omega}{v} \tag{4}$$

in a *braking* phase, and

$$\delta v = \frac{r\omega - v}{r\omega} \tag{5}$$

in a *traction* phase.

Wheel–rail contact forces in rolling conditions

A complete theoretical study of the adhesion in the micro-slip zone is described in by Kalker[1] and Johnson,[2] but its results cannot be used directly to obtain the wheel–rail model to be used for hardware in the loop (HIL) simulation of safety relevant subsystems like WSP systems, mainly for the following reasons:

- the accurate models described in previously cited studies are not adequate to simulate macroscopic sliding occurring with degraded adhesion conditions;
- considering real-time requirements for hardware-in-the-loop testing and the necessity of the simulation of many axles/contact points (at least four) involve the availability of limited computational resources and the preference for algorithms that can be solved in a known deterministic time;
- finally, for the application we are interested in, the model of the vehicle is planar, so tri-dimensional models considering multi-contact patches are too sophisticated in this case.

Given the magnitude of the tangential and the normal component of the contact force, numerical procedures are available[1] that evaluate the shape and the dimensions of the contact area and subdivide

it into the sliding and the adhesion zone.[16] This procedure is used for the analysis of the phenomena that occur in the contact area between two elastic bodies, which are rolling with respect to the other.

For small values of creepage, the relationship between the creepage and the creep force can be considered linear, so longitudinal F_x and lateral F_y forces and the moment M_z can be calculated according to Kalker theory

$$F_x = -f_{11}\xi$$
$$F_y = -f_{22}\eta - f_{23}\phi \qquad (6)$$
$$M_z = f_{23}\eta - f_{33}\phi$$

where f_{11}, f_{22}, f_{33}, f_{23} are the linear creep coefficients, depending on the contact ellipse semi-axis and on the material properties, their values are tabulated and can be found, for example, in Kalker.[1] The coefficients ξ, η and ϕ represent, respectively, the longitudinal, lateral and spin creepage components, and are defined as[17]

$$\xi = \frac{\mathbf{v}_c^r \cdot \mathbf{i}_r}{v_{ow}}$$
$$\eta = \frac{\mathbf{v}_c^r \cdot \mathbf{t}_r}{v_{ow}} \qquad (7)$$
$$\phi = \frac{\mathbf{\Omega}_w^r \cdot \mathbf{n}_r}{v_{ow}}$$

In the above expressions, $\mathbf{v}_c^r$ is the wheel speed at the contact point, $\mathbf{i}_r$ is the unit vector that identifies the rail longitudinal direction, $\mathbf{t}_r$ is the unit vector tangent to the contact surface and orthogonal to $\mathbf{i}_r$ (it identifies the lateral direction), $\mathbf{n}_r$ is the unit vector normal to the contact surfaces in the contact point, v_{ow} is the magnitude of the velocity of the wheelset centre of mass.

The tangential forces evaluated with this linear model have to be saturated, in order to approximate a limited known friction factor μ. The saturation of creep forces is performed according to the modified Jonshson–Vermeulen formulation,[17] by defining a coefficient k_s as

$$k_s = \begin{cases} \frac{\mu N}{F_R}\left[\left(\frac{F_R}{\mu N}\right) - \frac{1}{9}\left(\frac{F_R}{\mu N}\right)^2 - \frac{1}{27}\left(\frac{F_R}{\mu N}\right)^3\right] & \text{for } F_R \leqslant 3\mu N \\ \\ \frac{\mu N}{F_R} & \text{for } F_R > 3\mu N \end{cases}$$

$$(8)$$

where μ is the wheel–rail friction factor, N is the normal component of the force, $F_R = \sqrt{F_x^2 + F_y^2}$ is the total creep force and F^x and F^y are the creep forces in the x and y directions, respectively.

Wheel–rail contact forces when sliding is present

When the full contact zone is sliding, pure rolling conditions do not hold any more, and macroscopic sliding between the wheel and the rail occurs. In this phase, the adhesion coefficient depends on the absolute slip, defined in equation (4). The relationship between the adhesion coefficient μ and the absolute sliding Δw was investigated by many researchers because its behaviour is fundamental for the performance anti-skid and WSP devices.[6] This relationship is defined on the basis of experimental results, but, since macro-sliding occurs, for example, in the presence of contaminants in the contact area, the variability of adhesion coefficient due to non-homogeneous contact conditions is very high, and the identification of its dependence on slip is difficult.

To obtain a unique model, valid either for the micro-slip and the macro-slip ranges, it is necessary to express the adhesion factor μ as a function of the relative slip, given by the ratio between the absolute slip and the speed.

Since in this work, the longitudinal dynamics is analysed, the relative slip in this case is evaluated as the component of the above defined creepage in the longitudinal direction.

An example of relative slip/adhesion curve is presented in Boiteux,[6] and is shown in Figure 1. As can be seen, two curves are present: the continuous one refers to a *loss of adhesion*, i.e. to an increment of the slip, while the dashed curve is relative to a *recovery of adhesion*, i.e. to a decrement of the slip, and their typical shapes are clearly different.

The behaviour of the adhesion factor with degraded conditions seems to be affected also by vehicle speed, as confirmed by experimental tests and the literature.[6,7] The dependency on velocity has been often explained with the so-called *energetic* or *polishing* effect: degraded adhesion conditions are mainly due to contaminants present in the wheel–rail interface, when high sliding occurs, the energy dissipated by the friction produces localized heating that may partially destroy or remove contaminants; material from sliding surfaces is removed and the tribological features of the rolling surfaces are altered. As a consequence, the equivalent friction adhesion factor is modified. This is also called the *polishing* effect since the sliding of a wheel *clears* the rail from the contaminants, improving the adhesion conditions found by the following ones. This effect is often claimed to be responsible for the hysteresis behaviour of the adhesion factor during repeated cycles of contact losses. The cleaning effect mainly depends on the specific energy dissipated during the sliding per unit of length, which depends on vehicle speed; as a consequence, the effect due to energy dissipation produces an alteration of the adhesion factor that depends on speed and from the wear number associated with sliding. Relative sliding is a good index to evaluate this
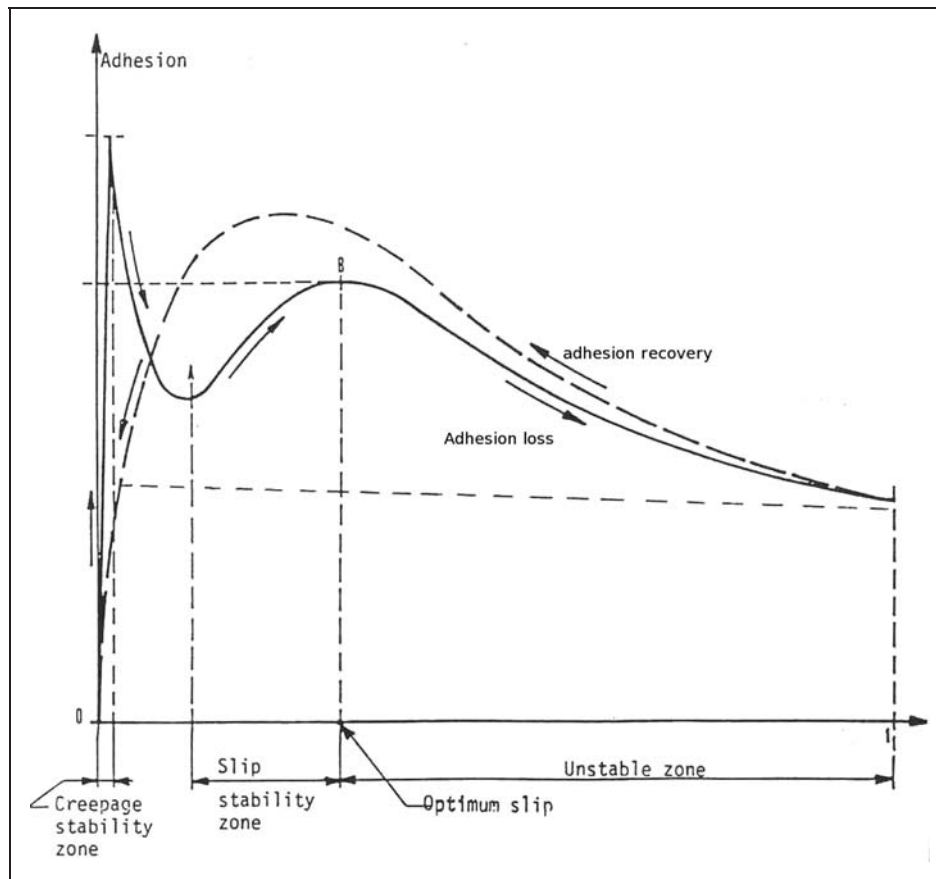
Figure 1. Typical qualitative behaviour of the slip/adhesion curve, adapted from Boiteux et al.[6]

phenomenon since it is approximately proportional to the specific energy dissipated over a unitary arc length. Other parameters, e.g. unmodelled contact force fluctuations due to the flexible behaviour of both wheel and rail, may contribute to modifying the behaviour of the adhesion factor with speed.

Data from test runs

The theoretical models and qualitative considerations described in the preceding section are useful for the comprehension of the wheel–rail contact phenomena, but do not give quantitative information on the adhesion curve.

In order to verify these qualitative behaviours and to obtain quantitative information, a set of experimental data, from a series of test runs, is analysed, to estimate, by means of a simplified dynamical model, the adhesion coefficient between the wheel and the rail. The experimental data used to identify the wheel–rail adhesion coefficient are obtained from a set composed of 27 braking tests,[11] conducted with a single vehicle, where the adhesion between the rail and the wheels is degraded by spraying a water-based solution of soap (cleonsol) on the wheel or on the rail.

The tests were originally devoted to verify the behaviour of WSP systems and were conducted according to Union Internationale des Chemins des

Fer (UIC) regulations on WSP homologation procedures.[18] In these tests, braking performance is evaluated in critical adhesion conditions, artificially reproduced. Braking performance is usually evaluated by means of braking stopping distance and deceleration; however, other parameters are often measured to obtain more detailed information on the system behaviour. The tests described in this paper were conducted with a single vehicle, a passenger coach named UIC Z1. In Figure 2(a), the device used to spray the solution of contaminants is shown. Alternatively, on some tests prescribed by UIC regulations, degraded adhesion conditions are realized by applying directly on the rails the solution of contaminants as shown in Figure 2(b).

The following measured values were available for this study:

- absolute vehicle speed v;
- vehicle wheel angular velocities ω_i, $i = 1, \ldots, 4$;
- pressure in the brake cylinder p_i, $i = 1, \ldots, 4$.

Each measurement is sampled with a time step of 2.4 ms, corresponding to 417 Hz. Train speed is measured by a radar Doppler sensor, whose signal is typically affected by high-frequency noise and spikes corresponding to track irregularities,[19] then it is filtered using a digital linear low-pass fourth-order filter with a cut-off frequency of 1.5 Hz. Wheel
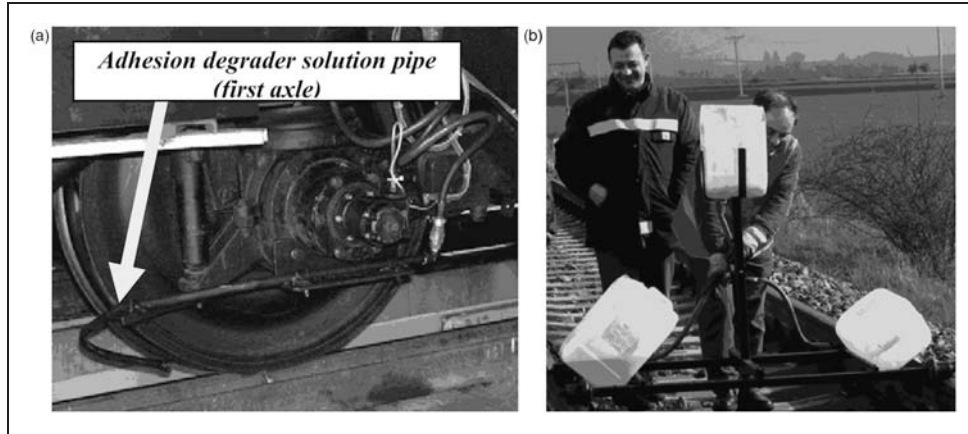
Figure 2. Degraded adhesion tests: (a) device used to produce degraded adhesion condition on the railway vehicle and (b) device used to produce degraded adhesion condition acting directly on the rails.[11]

velocities are measured with angular speed sensors, whose signals are affected by misalignment and quantization errors. Typically, their noise level is lower than the radar Doppler one, on the other hand, the dynamics of the wheel angular speed is faster than the vehicle one. In order to preserve the information content of axle speed measurements, angular speed sensors (tachometers) are filtered with a low-pass filter with a cut-off frequency of 4 Hz. Experimental data are elaborated using the MATLAB standard tools for signal processing.

Figure 3 shows one experimental braking test: Figure 3(a) shows the vehicle speed and the velocity of the first wheel during the braking, as a function of time, while Figure 3(b) shows the pressure in the corresponding brake cylinder, as a function of time as well. It is worth noting that the low adhesion and the intervention of the WSP system lead to an oscillating behaviour, both in the wheel tangential velocity and in the brake cylinder pressure. The amplitude and frequency of such oscillations depend on many factors, including the feature of the WSP system, the dynamical parameters of the vehicle, etc. The WSP system objective is to maintain the slip value in a range in which the adhesion coefficient is high: when the value of the braking force is too high, with respect to the available wheel–rail adhesion, the wheel begins to slide, and the sliding value increases rapidly (as can be seen, in these tests, it reaches values up to 5 m/s). The WSP device then modulates braking force, in order to reduce and control the slip value. Figure 4 shows, for a similar test, the vehicle speed and the wheel peripheral velocities relative to four wheels. In this figure, it is worth noting the different behaviour of the four wheel velocities, due to the different adhesion conditions met by the wheels, which determine different interventions of the WSP.

In these tests, the rail profile was the UIC 60, and the wheel was ORES1002; the profiles did not present significant wear, the track was straight and without turnouts.[20]

Simplified dynamic model

The dynamics of each wheelset can be described by the following differential equation, which is referred to as the simplified model of the wheel sketched in Figure 5,

$$T_i r = J\dot{\omega}_i + C_{f,i} \tag{9}$$

where T_i is the tangential component of the contact force acting on the ith axle, $\dot{\omega}_i$ is the axle angular acceleration, $C_{f,i}$ is the braking torque, r is the wheel radius and J is the axle moment of inertia. The braking torque $C_{f,i}$ has been assumed proportional to the brake cylinder pressure p_i

$$C_{f,i} = \alpha p_i \tag{10}$$

The proportionality coefficient α depends on the cylinder area, on the brake rigging ratio, on the brake efficiency and on the friction coefficient of braking materials, which in this study was assumed to be 0.35.[21] The friction factor of the brake pads is known from technical documentation of the pad maker, and it is also information available in the brake plant calculation, which is usually produced as part of the vehicle technical documentation. The brake pad friction factor can be easily verified or extrapolated from the braking test with full adhesion condition conditions exploiting the proportionality between vehicle deceleration and applied braking forces. From expression (9), T_i can be calculated as

$$T_i = \frac{1}{r}J\dot{\omega}_i + \frac{1}{r}\alpha p_i \tag{11}$$

Moreover, vehicle longitudinal deceleration is estimated with a simple derivative filter applied to train speed measurements. The vertical forces between vehicle body and bogies are estimated by means of a
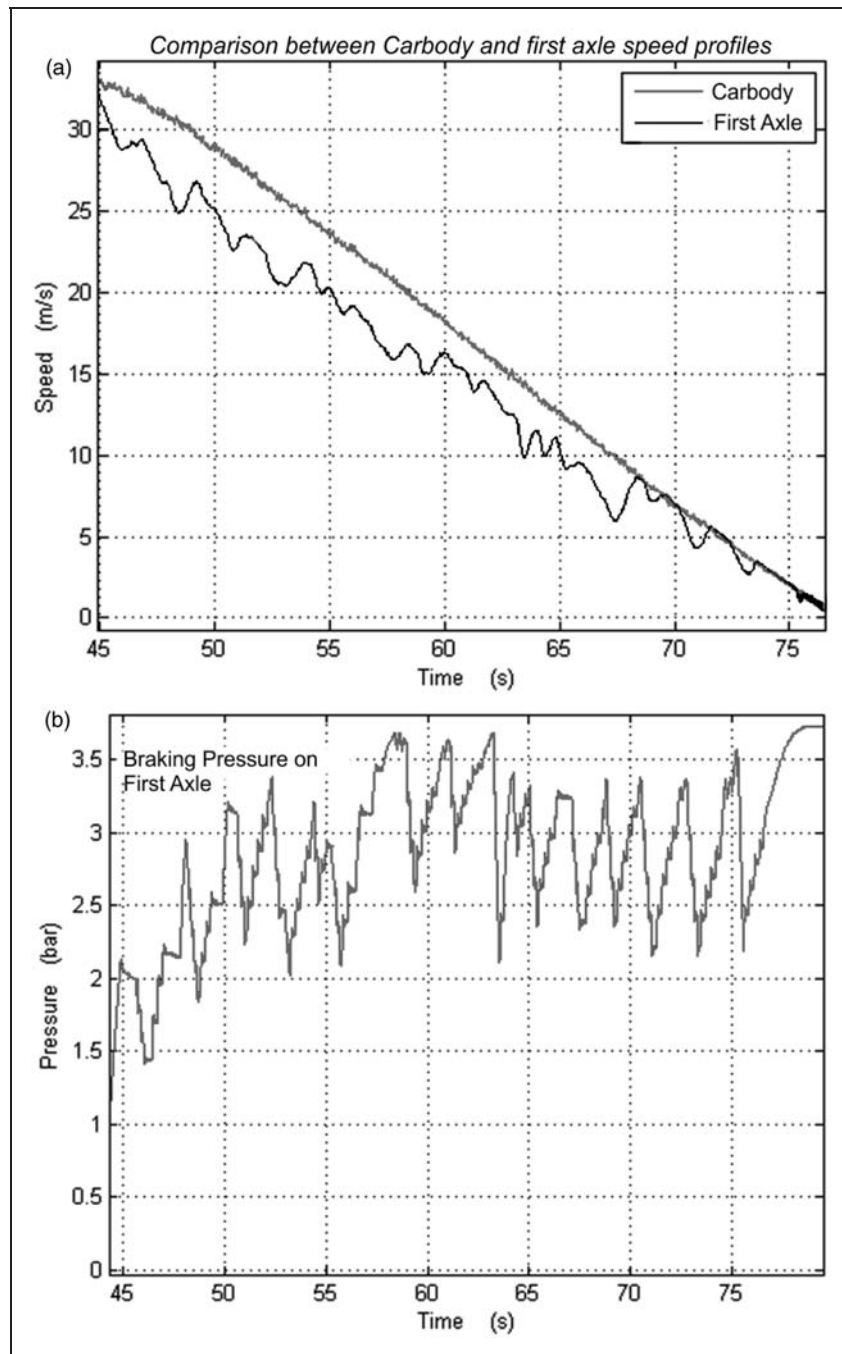
Figure 3. Example of data measured during a braking test: (a) comparison between train speed and wheel speed and (b) pressure on first brake axle.

simplified two-dimensional vehicle dynamic model, and then the normal load acting on each axle is evaluated. For example, the vertical force between the body and the front boogie can be evaluated as

$$N_{b1} = \frac{m_c \cdot g}{2} + \frac{m_c \cdot d \cdot (h_1 - h_b)}{l_1} \qquad (12)$$

where m_c is the car body mass, g is acceleration due to gravity, d is vehicle longitudinal deceleration and h_1, h_b, h_2, l_1 and l_2 are dimensions corresponding to the geometrical layout of the vehicle shown in Figure 6.

The vertical (normal) load acting on the front wheel of the front bogie can be evaluated as

$$N_1 = \frac{N_{b1} + m_{b1} \cdot g}{2} + \frac{m_{b1} \cdot dec \cdot h_2}{l_2} \qquad (13)$$

Vertical loads acting on the other wheels, namely N_2, N_3 and N_4, are calculated in a similar way.

Once the vertical and the longitudinal components of the contact force are estimated, the adhesion coefficient μ_i can be evaluated for each wheel and for each time sample. In Figure 7, the typical behaviour of the adhesion factor μ is shown, as a function of the slip
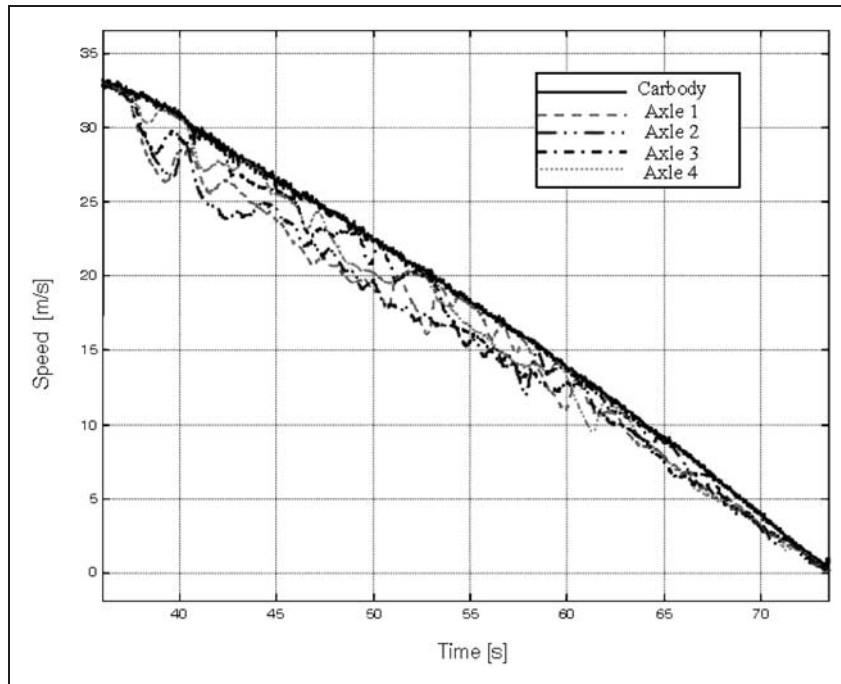
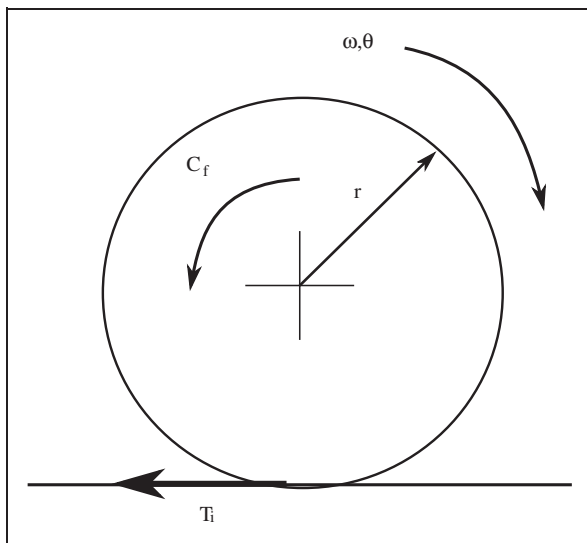**Figure 4.** Example of data measured during a braking test: vehicle speed and wheel velocities.

Figure 5. Forces and torques acting on a wheel during braking.

during single adhesion losses. The profile has been calculated using the experimental data corresponding to the test shown in Figure 4. In particular, curves $\mu_i(\Delta v)$ (index i represents the corresponding axle number) are evaluated using the following relationship

$$\mu_i = \frac{\alpha p_i + J_i \dot{\omega}_i}{N_i r_i} \qquad (14)$$

For example, in Figure 8 the adhesion curve obtained for the same axle with different braking speeds is shown: it is worth observing that the adhesion curve

depends on speed, as discussed, for example, in Polach.[7]

Definition of a model based on neural networks

As discussed in the preceding sections, the wheel–rail phenomenon is quite complex and depends on several uncontrollable and even unobservable parameters. On the other hand, simulation of degraded adhesion conditions is necessary to reproduce complex interactions that often arise among different mechatronic on-board systems and railway vehicle dynamics. Typical applications are the study and the simulation of WSP systems, anti-skid traction controls or odometry on-board subsystems.

The goal of the analysis described in this paper is to define a mathematical model able to describe, in a realistic but computationally efficient way, the behaviour of wheel–rail adhesion in critical environmental conditions, as those present in the experimental tests described in the preceding section.

The first variable that has to be taken into account in this study is the sliding Δv, furthermore, as outlined in the preceding sections, during cyclical sequences in which the wheel sliding is increased and decreased, the adhesion factor shows hysteresis. The time derivative of slip $\Delta \dot{v}$ is then useful to recognize the curve relative to *loss of adhesion*, i.e. to an increment of the slip, from the one relative to a *recovery of adhesion*, i.e. to a decrement of the slip.

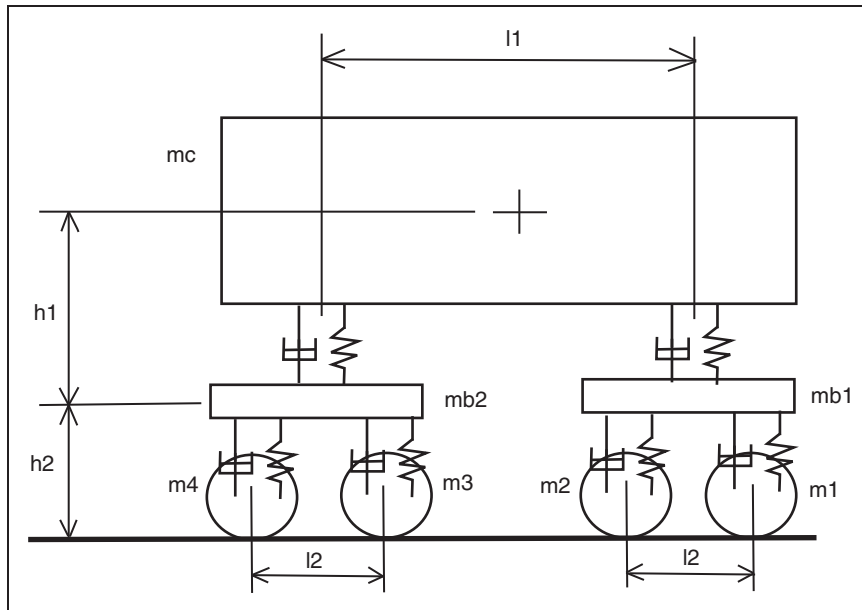In this work, a mathematical relationship between two inputs, which in our case, are the wheel slip

Figure 6. Simplified vehicle dynamic model of a railway vehicle in the longitudinal plane.
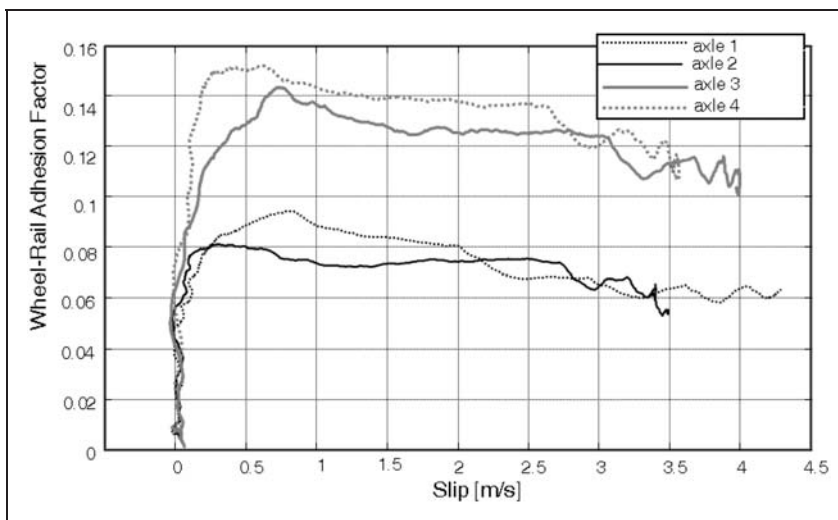

Figure 7. Wheel–rail adhesion factor as a function of slip calculated from degraded adhesion data of Figure 4, the curves were obtained elaborating data from the first loss of adhesion at the beginning of the braking phase.

Δv and its time derivative $\Delta \dot{v}$, and the adhesion factor μ, which is the output.

Mathematical models used to represent physical phenomena can be substantially divided into two main groups: deterministic or mechanistic models and data-driven models. The former are usually adopted when the phenomenon dynamics is quite simple and a limited set of experimental data are available, while, on the contrary, the latter ones are used when the system physics is uncertain or complex but several experimental measurements are available. Pugi et al.[22] presented a deterministic three-dimensional model that allowed the adhesion to be modelled also in critical conditions. They adopted different types of identification techniques to solve the problem. Data-driven models are also referred to as *black*

box models: a mathematical structure of the model is usually pre-defined, which depends on a series of parameters that are *tuned*, during an iterative process called *training* in order to replicate as precisely as possible the experimental data. Neural networks belong to this type of system identification methods.

In this paper, a simple and widely known type of neural network, the multi-layer perceptron, is adopted. A feed-forward neural network[23–25] consists of one or more layers of neurons. The latter layer is a defined output layer, while the others, when they are present, are referred to as hidden layers. Each layer is composed of a series of neurons, and each neuron is a simple dynamical system that applies a specific transfer function to a weighted sum of the inputs. The structure of the neural network is defined once the
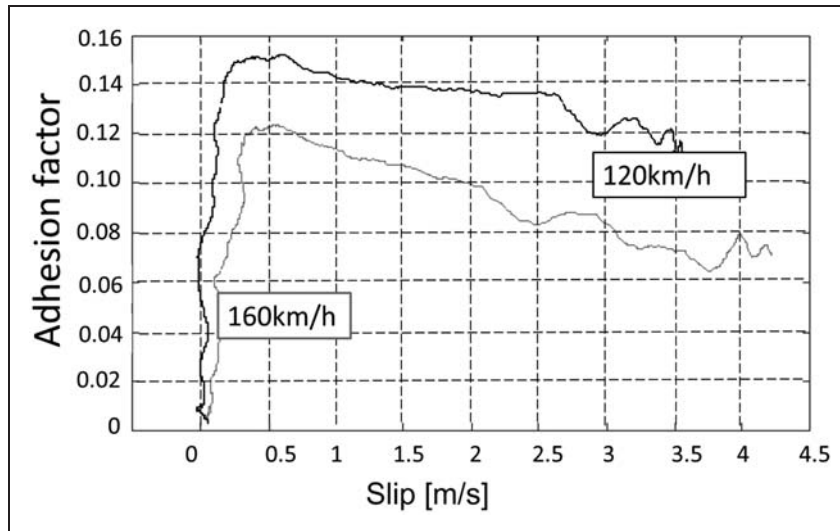
Figure 8. Slip curve from experimental tests of the second axle at 120 km/h and at 160 km/h the curves were obtained elaborating data from the first loss of adhesion at the beginning of the braking phase.
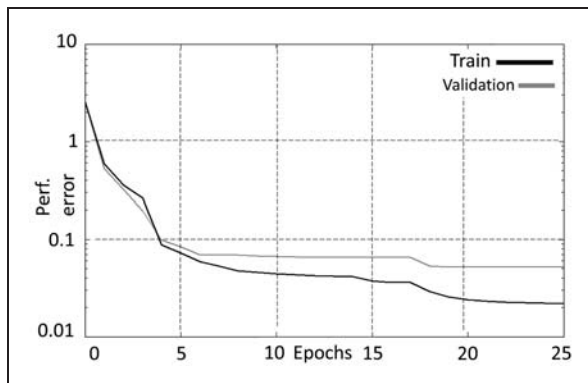

Figure 9. Error in the training and validation processes.

number of layers, the number of neurons for each layer, and the neuron transfer function are defined. The identification of a function using data-driven techniques in general requires three steps. The first step is the collection of reference data; each datum is a vector that contains an input vector and the corresponding measured output vector. The available data are usually divided in two subsets: the *training data set* and the *validation data set*. The first one is used for the iterative optimization of network parameters (training), while the second one is used to evaluate system performance. In our application, for the training phase, the second axle data were used, while for the validation, we used the third axle ones. This solution was adopted for convenience, even if it could seem better to choose, for the data sets, measurements from all the wheels. However, since the vehicle used to perform the tests is symmetric, and the tests are conducted in two different directions, we could assume that the data sets from the second and third wheels are quite similar.

Then the network's architecture (organization of neurons in the network and definition of the activation function for each neuron) is defined. Finally, the network is *trained*: reference data are submitted to the network and the values of parameters are updated in an iterative process in order to minimize the *error* between the network output and the desired output. The error can be defined in several ways; usually a measurement of the distance is used, in this paper, we adopted the mean square error. The chosen architecture is a multi-layer perceptron, using in the training process, the Levenberg–Marquardt algorithm.[23–25]

The performance of a neural network depends on its architecture; for the examined problem, double-layer networks have been chosen, with hyperbolic tangent activation functions in the hidden layer and linear activation functions in the output layer. This type of architecture has been chosen since it is simple and widely adopted in the identification of non-linear systems starting from noisy measurements.

Some tests were performed to find the optimal number of neurons in the hidden layer: if the number of neurons is too low, the model is too simple and is not able to reproduce the complexity of the physical phenomenon. On the other hand, increasing the number of neurons, the system complexity obviously increases, also from the computational point of view. Furthermore, if the network is too complex, it is no more able to capture the physics of the system, but rather tends to *copy* the input/output experimental pairs, which usually are affected by measurement noise, and the system outputs may be not realistic. Some tests showed that in the presented case, the optimal size of the hidden neuron layer is 10.

At the end of the training process, the neural network defines substantially the function between the
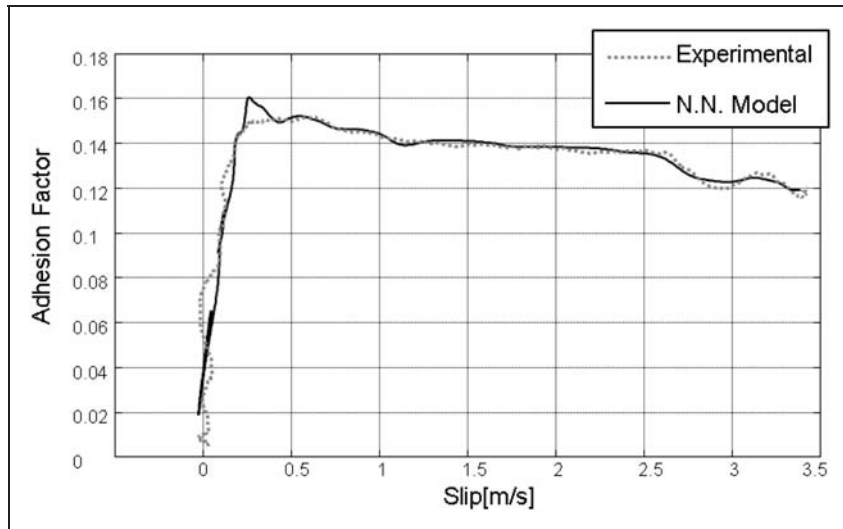
Figure 10. Slip curve of second axle: comparison between the neural network (N.N.) output and experimental data.
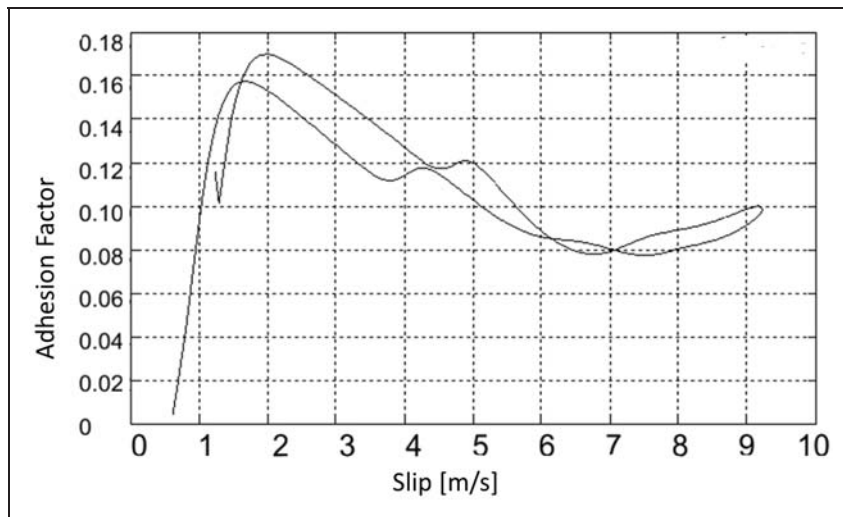

Figure 11. Complete slip curve (simulated), obtained at a speed of about 120 km/h.

sliding (and its time derivative) and the adhesion coefficient. Results are then analysed and verified using, as inputs, experimental data not included in the training process.

Figure 9 shows the behaviour of the relative error for the training and validation data sets as a function of the number of training epochs (i.e. number of iterations in the training process). The diagram shows a good mutual accordance and a quite similar dependency from the number of epochs between the different data sets, this result confirms that the training and validation data sets have similar information contents.

Results

Figure 10 shows, for a test included in the validation data set, a comparison between the experimental and the model predicted adhesion values. As can be observed from the figure, the neural network based model is able to reproduce the experimental data with a good approximation. This test was obtained by giving to the neural network identification model the inputs from an experiment and observing the corresponding output. Since the input data are those from experimental measurements, the output of the identification model presents some oscillations and some sharp points.

The behaviour in the first part of the diagram, corresponding to small sliding values, is approximately linear, but presents some irregularities due to the measurement errors. Actually, in this part of the diagram, the identification model reliability is not very high, because of the unreliability and noise in the experimental measurements. In an implementation of the model devoted to reproduce the dynamics of a railway vehicle, this part could be substituted by a

linear model as described in the subsection on wheel–rail contact forces in rolling conditions.

The obtained mathematical model based on neural networks is then verified by giving regular patterns and smooth functions as inputs. For example, Figure 11 shows the results obtained by linearly increasing the sliding from zero to a maximum value of about 9 m/s and then decreasing it linearly up to zero. The time derivative of the sliding in this example is then composed of two constant parts, the first positive and the second negative. This example shows how the obtained model can reproduce the typical shape of a simulated cycle composed of a loss of adhesion and a following recovery of rolling conditions, the typical hysteresis behaviour of the adhesion factor is evident. In the diagram, the part of the curves relative to small sliding values (around zero) is not displayed, since the identification procedure is not very reliable in this part, as previously discussed.

Conclusions

Identification of adhesion behaviour in the wheel–rail contact is a multi-faceted phenomenon that is hard to investigate. This paper analyses the problem of the adhesion identification in braking, analysing a reachable models that correlates slip and adhesion coefficient. The numerical estimation of the adhesion coefficient from a set of data tests allowed a series of absolute slip/adhesion curves to be obtained(for each axle relative to different train speeds). Then, an identification of the adhesion coefficient using a standard neural network procedure was implemented: it permitted the definition of a mathematical model for the evaluation of the adhesion coefficient as a function of the wheel sliding. In addition, the obtained model produces results compliant with the main properties of the observed phenomenon, e.g. the different behaviour corresponding to loss of adhesion and recovery of adhesion. Since the simulated phenomena are also dominated by stochastic disturbances, clearly, a perfect fit of experimentally measured time histories is not possible.

The proposed adhesion model is limited to a bi-dimensional approach that constrains possible applications to planar vehicle models which are often used for real-time simulation on HIL test rigs such as those described in Pugi et al.[11] or to full-scale roller rigs such as those described in Allota et al.[12] and Malvezzi et al.[13] Further work will be devoted to produce degraded adhesion models able to reproduce a near to realistic behaviour also on multi-patch, three-dimensional contact models usually used for multibody simulations.

References

1. Kalker JJ. *Three-dimensional elastic bodies in rolling contact*. Dordrecht: Kluwer Academic Publishers, 1990.
2. Johnson KL. *Contact mechanics*. Cambridge: Cambridge University Press, 1989.
3. Zhu Y, Olofsson U and Söderberg A. Adhesion modeling in the wheel–rail contact under wet condition using measured 3D surfaces. In: *22nd international symposium on dynamics of vehicles on roads and tracks*. IAVSD, Manchester, UK, 14–19 August 2011.
4. Fries R, Urban C and Wilson N. Modeling friction modifier and lubricant characteristics for rail vehicle simulations. In: *22nd international symposium on dynamics of vehicles on roads and tracks*. IAVSD, Manchester, UK, 14–19 August 2011.
5. Voltr P and Lata M. Dynamical behaviour of a locomotive drive system at the adhesion limit-experiment and simulation. In: *22nd international symposium on dynamics of vehicles on roads and tracks*. IAVSD, Manchester, UK, 14–19 August 2011.
6. Boiteux M, Cadier M, Kling J, et al. Adhérence en freinage et anti-enrayeurs. Document technique DT257 (B164), Office de Recherches et d'Essays de L'Union Internationale des Chemins de fer, July 1992.
7. Polach O. Creep forces in simulations of traction vehicles running on adhesion limit. *Wear* 2005; 258: 992–1000.
8. Goodall R and Guy C. Low adhesion estimation. In: *Procedings of railway condition monitoring*, Birmingham, UK, 2006.
9. Tomeoka M, Kabe N, Tanimoto M, et al. Friction control between wheel and rail by means of on-board lubrication. *Wear* 2002; 253: 124ô129.
10. Wang WJ, Shen P, Song JH, et al. Experimental study on adhesion behaviour of wheel/rail under dry and water conditions. *Wear* 2011; 271: 2699–2705.
11. Pugi L, Malvezzi M, Tarasconi A, et al. In: Taylor and Francis (eds) *Simulation of WSP systems on MI-6 test rig, vehicle system and dynamics*. vol. 44, supplement 2006, pp.843–852. ISBN 978-0-415-43616-8.
12. Pugi L, Malvezzi M, Tarasconi A, et al., Simulation of WSP systems on MI-6 test rig, Vehicle System Dynamics, Taylor and Francis (eds), vol. 44, supplement 2006, pp.843 -852. ISBN 978-0-415-43616-8.
13. Malvezzi M, Allotta B and Pugi L. Feasibility of degraded adhesion tests in a locomotive roller rig. *Proc IMechE, Part F: J Rail and Rapid Transit* 2008; 222(1): 27–43.
14. Watanabe T and Yamanaka A. Adhesion phenomena and optimization of readhesion control for high speed trains with wheel–rail adhesion prediction. In: *Proceedings of the world congress on railway research*, 1997, pp.359–364.

15. Andresen E and Grimm R. Identification of rail-wheel adhesion. In: *SPEEDAM symposium on power electronics, electrical drives, automation and motion*. 2000, pp.C1 19–24.

16. Vollebregt EAH, Kalker JJ and Wang G. *CONTACT 93 Users Manual*. VORtech Computing, Industrial and Scientific Computing, July 1992. revised March 1994.

17. Dukkipati RV and Amyot JR. *Computer aided simulation in railway dynamics*. Marcel Dekker, 1988.

18. Fiche 541-05 *Brakesspecifications for the construction of various brake parts, wheel slide protection device*. 2nd edn. November 2005.

19. Pugi L, Rinchi M, Violani M, et al. Development of an experimental rig for HIL testing of railway radar speed sensors. In: *Railway Engineering*. 6–7 July 2004.

20. Esveld C. *Modern railway track*. 2nd edn. Delft University of Technology, 2001.

21. Pugi L. *Progettazione e Realizzazione di un Banco Prova per lo studio e la omologazione di sistemi di odometria ferroviari*. PhD Thesis. University of Bologna, Italy, 2003.

22. Pugi L, Ridolfi A, Malvezzi M, et al. Three-dimensional modelling of wheel-rail degraded adhesion conditions. In: *22nd international symposium on dynamics of vehicles on roads and tracks*. IAVSD, Manchester, UK, 14–19 August 2011.

23. Demuth H and Beale M. *Neural network toolbox for use with MATLAB*. The Mathworks, Inc.

24. Hagan MT, Demuth HB and Beale MH. *Neural network design*. Boston, MA: PWS Publishing, 1996.

25. Hagan MT and Menhaj M. Training feedforward networks with the Marquardt algorithm. *IEEE Trans on Neural Networks* 1994; 5(6): 989–993.

Appendix 1

Notation

dec (m/s^2)	train deceleration
$f_{11}, f_{22}, f_{33}, f_{23}$	linear creep coefficients
$\mathbf{i}_r$	unit vector that identifies longitudinal direction
g (m/s^2)	gravity acceleration
h_1, h_2, h_b, l_2 (m)	vehicle dimensional features, shown in Figure 6
k_s	coefficient for the tangential contact force saturation
m_{b1}, m_{b2} (kg)	bogie masses
m_c (kg)	car body mass
m_i (kg)	mass of each wheel
$\mathbf{n}_r$	unit vector normal to the contact surfaces in the contact point
p_i (Pa)	pressure at the ith brake cylinder
r (m)	wheel radius
r_f (m)	wheel braking radius
$\mathbf{t}_r$	unit vector tangent to the lateral direction
v (m/s)	train speed
v_{ow} (m/s)	magnitude of the velocity of the wheelset centre of mass
$\mathbf{v}_c^r$ (m/s)	wheel speed at the contact point
C_f (Nm)	braking moment at the wheel
$C_{f,i}$ (Nm)	braking moment at the ith wheel
F_x (N)	contact force component in the longitudinal direction
F_y (N)	contact force component in the lateral direction
F_R (N)	resultant of longitudinal and lateral contact force components
J_i (kg m^2)	wheelset moment of inertia
N (N)	normal component of the contact force
N_i (N)	normal contact force at the wheel i
N_{bi} (N)	vertical force between the car body and the ith bogie
T (N)	tangential component of the contact force
T_i (N)	tangential contact force at the wheel i
α	proportionality coefficient between brake pressure and brake torque
μ	adhesion coefficient
ξ, η and ϕ	longitudinal, lateral and spin creepage
δv (m/s)	relative slip
ω (rad/s)	angular wheel velocity
ω_i (rad/s)	angular velocity of the ith wheel
$\dot{\omega}$ (rad/s^2)	angular wheel acceleration
$\dot{\omega}_i$ (rad/s^2)	angular acceleration of the ith wheel
Δv (m/s)	absolute slip